Applied Surface Science 263 (2012) 345–351

Contents lists available at SciVerse ScienceDirect

Applied Surface Science

journal homepage: www.elsevier.com/locate/apsusc

Enhanced photocatalytic decomposition of methylene blue by the heterostructure of PdO nanoflakes and TiO_2 nanoparticles

Chien-Jung Huang, Fu-Ming Pan*, I-Chun Chang

Department of Materials Science and Engineering, National Chiao Tung University, 1001 Ta Hsueh Road, Hsinchu, 30010 Taiwan, ROC

ARTICLE INFO

Article history:
Received 27 July 2012
Received in revised form
12 September 2012
Accepted 12 September 2012
Available online 29 September 2012

Keywords:
PdO
TiO_2
Heterostructure
Methylene blue
Photocatalysis

ABSTRACT

We prepared PdO nanoflakes by reactive sputter deposition to form a heterostructure with TiO_2 nanoparticles on the SiO_2 substrate for the study of photocatalytic decomposition of methylene blue (MB) molecules. Although the PdO nanoflake has little photocatalytic activity toward MB decomposition, the PdO/TiO_2 heterostructure has a photocatalytic activity toward MB decomposition under UV light illumination as large as twice that of bare TiO_2 nanoparticles. The enhancement in the photocatalytic activity is ascribed to the fast photogenerated carrier separation resulting from the potential barrier formed at the heterojunction between the two oxide semiconductors. Although PdO nanoflakes can be photoexcited under visible light illumination, the PdO/TiO_2 heterostructure exhibits little photocatalytic activity toward the MB decomposition.

1. Introduction

Titanium dioxide (TiO_2) is a n-type semiconductor with a bandgap of ~3.2 eV [1,2]. Because of its high chemical stability, low toxicity and low cost, TiO_2 has been widely studied for various environmental applications, such as energy conversion of water splitting [3–5], methanol oxidation [6–8], environmental protection [9–11] and dye-sensitized solar cells [12–14]. The photocatalytic activity and light absorption of TiO_2 can be improved by many sample treatment methods, such as selective syntheses of TiO_2 nanostructures with high-energy surfaces [15] and preparation of nitrogen-doped TiO_2 catalysts [16,17]. However, TiO_2 is considered far from a practical photocatalyst due to the lack of visible light absorption and a fast recombination rate of photogenerated carriers [1,18]. In the past decades, TiO_2 based heterojunction structures have been extensively studied for the improvement in the photocatalytic performance of TiO_2 because the junction barrier can effectively separate photogenerated electron–hole (e–h) pairs and thus decrease the carrier recombination rate [1,19]. For instance, noble metals, such as Pt [20,21] and Au [22], have been employed to form schottky barriers with TiO_2. Another and more popular approach is to form a heterojunction of TiO_2 with semiconductors of narrower bandgap, such as CdS [23] and Cu_2O [24] to facilitate fast charge separation and thereby reduce charge carrier recombination [23–25]. In addition to the increase in the lifetime of photogenerated e–h pairs, it is generally believed that these narrow bandgap semiconductors, which usually have a light absorption spectrum covering the visible light range, can also improve the solar energy utilization, resulting in a better photocatalytic performance of TiO_2.

In this study, we prepared PdO nanoflakes by reactive sputter deposition to form a heterostructure with TiO_2 nanoparticle and study the photocatalytic activity of the PdO/TiO_2 heterostructure toward organic decomposition. PdO is a p-type semiconductor with a small bandgap energy of ~0.8–2.2 eV [26–28]. In our previous study, the PdO nanoflakes have a strong absorption maximum at ~620 nm and exhibit a very sensitive photoresponse behavior under UV and visible (UV–vis) light illumination. The formation of the p–n junction between the PdO nanoflake and the TiO_2 nanoparticle is expected to enhance the photocatalytic activity of TiO_2 because the built-in field at the heterojunction can effectively separate photogenerated electrons and holes, and thus increase the lifetime of e–h pairs. A previous study by Ismail demonstrated that PdO–TiO_2 nanocomposites could improve the photocatalytic activity of TiO_2 toward methanol oxidation [29]. We used methylene blue (MB) aqueous solution as the test reagent for the study because MB is a typical organic dye in textile effluents [30,31] and the MB concentration can be easily monitored by optical absorption spectroscopy. The study result shows that the PdO/TiO_2 heterostructure can significantly enhance the photocatalytic activity of TiO_2 nanoparticles toward MB decomposition

* Corresponding author. Tel.: +886 3 5131322; fax: +886 3 5724727.
E-mail address: fmpan@faculty.nctu.edu.tw (F.-M. Pan).

0169-4332/$ – see front matter © 2012 Elsevier B.V. All rights reserved.
http://dx.doi.org/10.1016/j.apsusc.2012.09.058

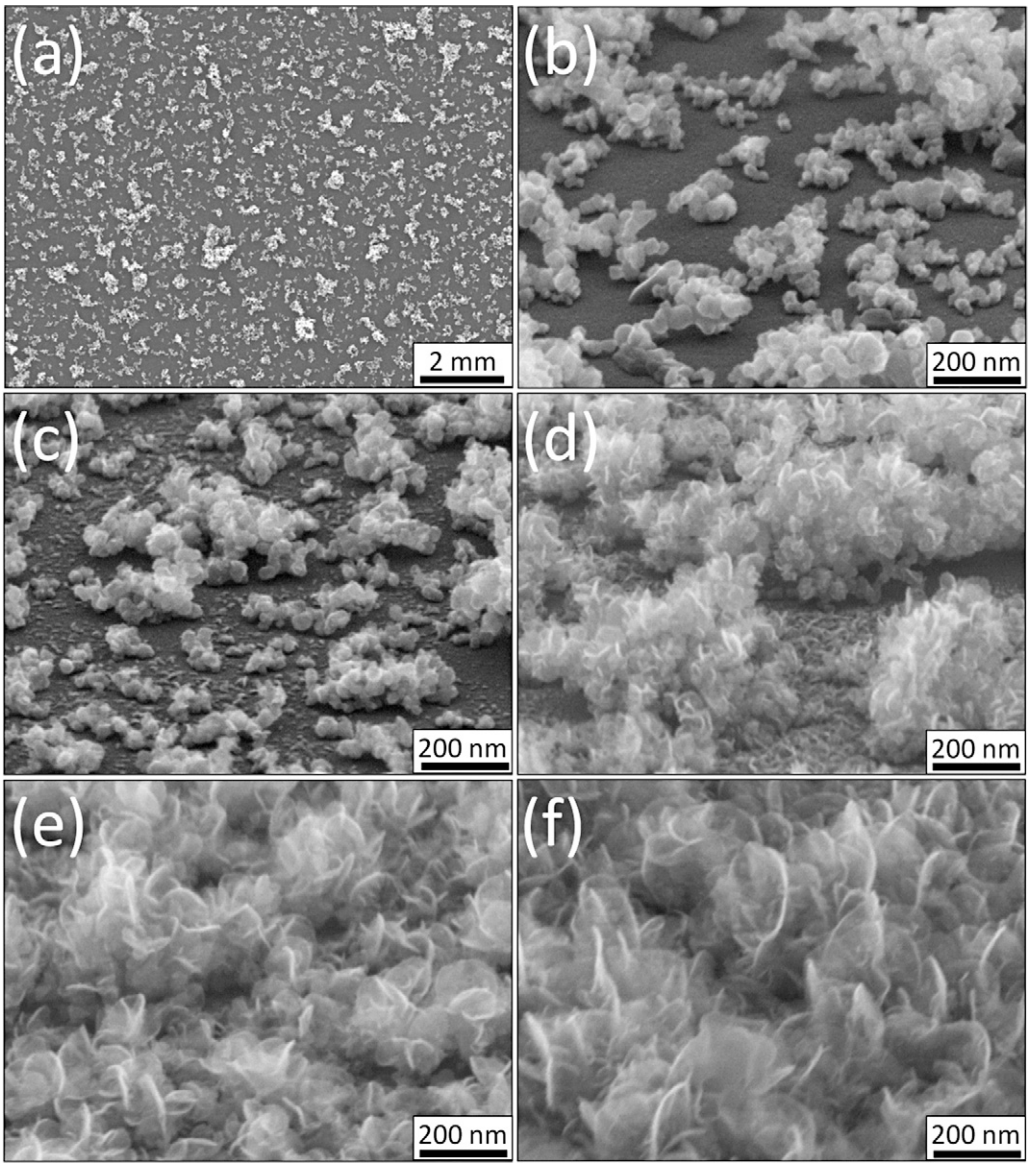

Fig. 1. (a) SEM images of P-25 TiO_2 nanoparticles spun on the SiO_2 substrate, and SEM images of the PdO/TiO_2 heterostructures prepared with different PdO deposition times: (b) 1 min, (c) 3 min, (d) 4 min, (e) 8 min, and (f) 12 min.

under UV light illumination, but is inactive in the visible light regime.

2. Experimental

The PdO/TiO_2 heterostructure was prepared by depositing PdO nanoflakes on TiO_2 nanoparticles, which were dispersed on a 150 nm thick SiO_2 thin film thermally grown on a 6-in. p-type Si (1 0 0) wafer. Since SiO_2 has little photocatalytic activity toward MB degradation, the observed photocatalytic phenomenon can be ascribed mainly to the TiO_2 nanoparticles. To disperse TiO_2 nanoparticles on the SiO_2 substrate, we first prepared the suspension solution of commercial Degussa TiO_2 powders (P-25) in ethanol at room temperature in an ultrasonic bath. The P-25 suspension solution was then spun on the substrate, followed by drying at 120 °C. The deposition of PdO on the P-25 TiO_2 nanoparticles was carried out at room temperature in a radio frequency magnetron sputter deposition system, using a palladium target of 99.99% purity, with a gas mixture of Ar (20 sccm) and O_2 (20 sccm) at a working pressure of 9×10^{-3} torr and a rf power of 50 W. A more detailed description about the PdO deposition process has been previously reported [32,33]. Five PdO/TiO_2 heterostructure thin films with different PdO deposition times were prepared; they are denoted by TiO_2–PdO-1, TiO_2–PdO-3, TiO_2–PdO-4, TiO_2–PdO-8 and TiO_2–PdO-12 with the number at the end representing the deposition time in minute. The as-prepared PdO/TiO_2 heterostructure thin film was annealed at 400 °C for 2 h to improve the crystallinity of the PdO nanoflakes. The surface morphology of the PdO/TiO_2 thin films was examined by scanning electron microscopy (SEM, JEOL JSM-6500F). X-ray diffractometry (XRD, PANalytical X'Pert Pro) and transmission electron microscopy (TEM, JEOL JEM-2100F) were used to study the microstructure of the PdO nanoflake thin film.

The variation in the MB concentration in an aqueous solution due to photodegradation is usually studied by UV–vis absorption spectroscopy [34]. In this study, the MB concentration was evaluated using a Hitachi U-3900H UV–vis spectrophotometer by measuring the absorption peak at 665 nm. The photocatalyst sample was cut into a square shape with an area of ~2 cm × 2 cm. An aqueous MB solution of 1×10^{-5} M was used as the test reagent in

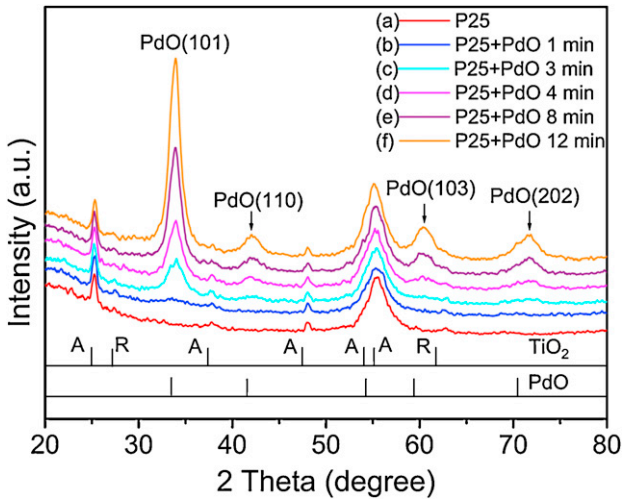

Fig. 2. XRD spectra of (a) the P-25 sample, and the PdO/TiO_2 heterostructures prepared with different PdO deposition times: (b) 1 min, (c) 3 min, (d) 4 min, (e) 8 min, and (f) 12 min.

the study. Fifty milliliters of the MB solution was transferred to a cuboid quartz tube and, prior to light irradiation, the solution was stirred for 30 min in dark to stabilize MB adsorption on the photocatalyst and the wall surface of the test tube. A 250 W Xe lamp was used as the UV/vis light source. An edge filter (λ < 420 nm) was used when visible light illumination is required.

3. Results and discussion

Fig. 1 shows SEM images of the P-25 TiO_2 sample and the PdO/TiO_2 heterostructure prepared with different deposition times and annealed at 400 °C for 2 h. Spin-deposited P-25 TiO_2 nanoparticles are well dispersed on the SiO_2 substrate as shown in Fig. 1(a). The uniform dispersion of P-25 nanoparticles ensures that PdO/TiO_2 heterostructures prepared with different PdO deposition time has a constant P-25 loading. After PdO deposition of 1 min, the TiO_2–PdO-1 sample shows little change in the surface morphology compared with the bare P-25 sample (Fig. 1(b)). This is because deposited PdO grains, which is around 2–3 nm in size as revealed by TEM analysis discussed below, is too small to be perceived in the SEM image. According to Fig. 1(c), most islands grown on the TiO_2–PdO-3 sample exhibit flake-like feature, indicating that PdO nanoflakes begin to grow on the sample surface at a deposition time of 3 min. The density and the size of PdO nanoflakes increase with the deposition time; nearly all the P-25 nanoparticles on the TiO_2–PdO-8 and TiO_2–PdO-12 samples are covered by PdO nanoflakes as shown in Fig. 1(e) and (f), respectively. Fig. 2 shows XRD spectra of the P-25 and the PdO/TiO_2 heterostructure samples. Before the PdO deposition, the bare P-25 TiO_2 sample shows an XRD spectrum typical for commercial Degussa P-25 TiO_2 powders. The TiO_2–PdO-1 heterostructure does not show apparent diffraction peaks associated with PdO. However, for the heterostructure with the PdO deposition time larger than 1 min, the intensity of diffraction peaks due to the PdO tetragonal lattice increases with the PdO deposition time. The strong and well resolved XRD peaks indicate that PdO nanoflakes grown in the heterostructure samples has a good crystallinity after the thermal anneal.

Fig. 3 shows TEM images of the P-25 and the as-prepared PdO/TiO_2 heterostructures with different PdO deposition times. The TEM specimens were prepared by scratching off the PdO/TiO_2 composite from the sample with a tweezers. According to Fig. 3(a), the P-25 TiO_2 nanoparticles have a size of ~25–40 nm. After the PdO deposition of 1 min, nanograins with a size of ~2–3 nm uniformly distribute over the P-25 nanoparticle as shown in the inset of Fig. 3(b). The high resolution TEM (HRTEM) image shown in Fig. 4(a) indicates that the nanograins are PdO nanocrystals as revealed by the lattice fringe associated with the PdO (0 0 2) plane, which has a lattice spacing of 0.267 nm. The growth of ultrathin PdO nanoflakes on P-25 nanoparticles becomes obvious for samples with the PdO deposition time longer than 1 min. The TEM images of Fig. 3(c) and (f) clearly show that PdO thin sheets are randomly adhered to P-25 nanoparticles. Fig. 4(b) shows the HRTEM image of a selected area in Fig. 3(f), which shows nanoflakes interweaving with each other. The lattice spacings marked in the HRTEM image correspond to (1 0 3) and (0 0 2) planes of the PdO tetragonal lattice structure. We have previously found that PdO nanoflakes grown on the SiO_2 substrate have a single crystalline structure [32]. The ultrathin sheets in the PdO/TiO_2 samples are likely single-crystalline PdO nanoflakes as well.

The UV–vis diffuse reflection absorption spectra of the bare P-25 sample and the five PdO/TiO_2 heterostructures are shown in Fig. 5. P-25 nanoparticles can only absorb light of wavelength shorter than ~380 nm because of its wide bandgap. After the PdO deposition, the absorption wavelength of the PdO/TiO_2 heterostructures extends to ~600 nm and the absorbance increases with the PdO deposition time. The extension of the light absorption to the lower energy region for the heterostructure samples must result from the visible light absorption by PdO nanoflakes.

The photocatalytic activity of PdO/TiO_2 heterostructures toward methylene blue degradation was also studied by UV–vis absorption spectroscopy. Prior to light irradiation, the solution was stirred for 30 min in dark so that adsorption equilibrium of MB on the photocatalyst samples and the wall surface of the test tube can be reached. During the UV–vis illumination, a gradual bleaching of the solution occurred indicating the occurrence of MB decomposition. In addition to the bleaching, gaseous bubbles, which are likely gaseous products of the MB decomposition (such as CO_2), developed on the surface of the PdO–TiO_2 photocatalyst samples. Fig. 6(a) shows time-dependent absorption spectra of MB solutions in the presence of PdO–TiO_2-4 under UV–vis light illumination. When the illumination time increases, the intensity of the light absorption in the range between 450 and 750 nm greatly decreases, indicating that a considerable amount of MB molecules decomposes under the illumination condition. Self-photolysis of MB in aqueous solutions can be initiated by light with wavelengths below 350 nm and above 480 nm [34]. However, the large decrease in the MB concentration with the illumination time is primarily due to MB decomposition photocatalyzed by the heterostructure. Fig. 6(b) shows the residual MB concentration as a function of the illumination time for the control MB solution and the MB solution in the presence of the PdO/TiO_2 heterostructure samples. The residual MB concentration is defined herein by C/C_0, where C and C_0 are the residual and the initial concentrations of MB, respectively. In the absence of the photocatalyst, the MB concentration is reduced by ~35% as a result of the self-photolysis of the MB solution. The bare PdO thin film exhibits little photocatalytic activity toward MB decomposition. On the other hand, the bare P-25 sample greatly enhances the MB photodegradation; about 71% of MB is decomposed after four hours of UV–vis light illumination. When PdO/TiO_2 heterostructure samples are present in the MB solution, the MB photodegradation rate can be much further enhanced. Among all the tested PdO/TiO_2 photocatalysts, TiO_2–PdO-4 has the highest photodegradation efficiency (defined by $1 - C/C_0$) and TiO_2–PdO-12 has the smallest. After four hours of UV–vis light illumination, the MB photodegradation efficiency for the TiO_2–PdO-1, TiO_2–PdO-3 and TiO_2–PdO-4 photocatalysts are ~89.7%, ~92.6% and ~96.1%, respectively. When the MB self-photolysis under the UV–vis light illumination is taken into account, the TiO_2–PdO-4 heterostructure has a photodegradation efficiency about twice as large as the bare

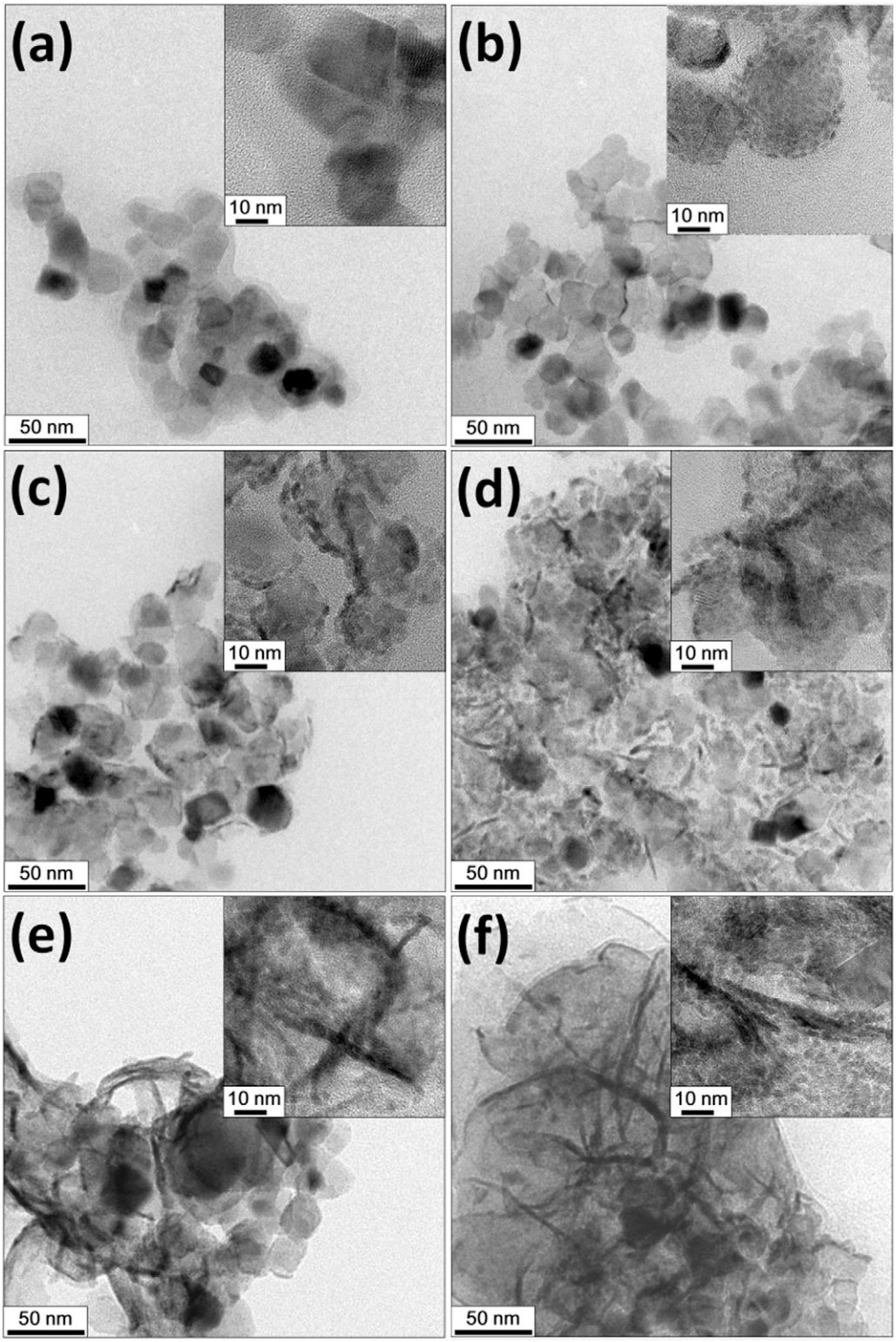

Fig. 3. TEM images of the P-25 sample (a), and the PdO/TiO_2 heterostructures prepared with different PdO deposition times: (b) 1 min, (c) 3 min, (d) 4 min, (e) 8 min, and (f) 12 min. The insets in (a)–(f) are the corresponding enlarged TEM images.

P-25 sample. However, further increase in the PdO loading does not accordingly increase the photocatalytic activity of the PdO/TiO_2 heterostructure. When the TiO_2–PdO-8 and TiO_2–PdO-12 samples are used to catalyze MB photodecomposition, the MB concentration is reduced by 76% and 72%, respectively. The less photodegradation efficiency for the two heterostructures is likely due to that the UV light absorption by P-25 nanoparticles is retarded by the heavily deposited PdO nanoflakes, which can effectively absorb incident UV photons. Besides, the heavy PdO nanoflake deposition for the two samples results in a smaller bare TiO_2 surface area, leading to fewer reaction sites for MB photocatalytic decomposition.

To study if PdO could enhance the photocatalytic activity of TiO_2 in the visible light range, we cut off the UV light from the xenon

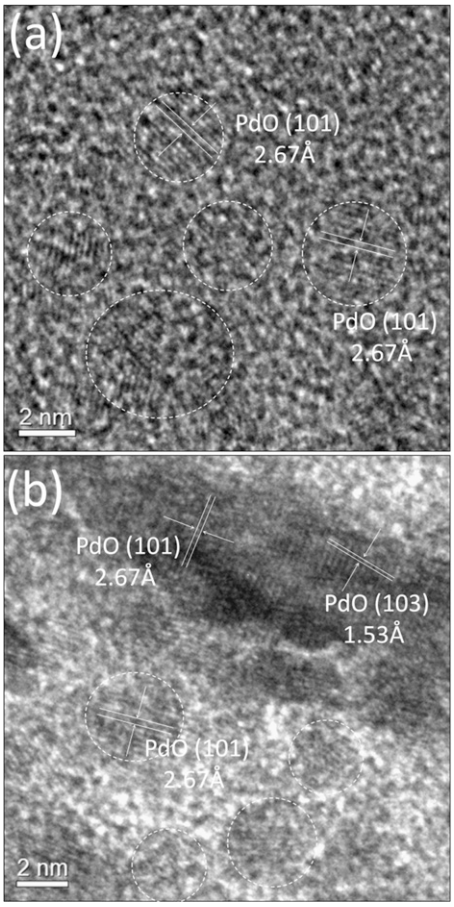

Fig. 4. HRTEM images of (a) the TiO_2–PdO-1 and (b) the TiO_2–PdO-12 heterostructures.

lamp with a 420 nm edge filter and repeated the MB photodegradation test under the same experimental condition as described above. As shown in Fig. 6(c), all the test samples demonstrate little photocatalytic activity toward MB degradation. The observed decrease in the MB concentration is due to self-photolysis of MB molecules under the visible light illumination. The visible light illumination experiment suggests that the PdO/TiO_2 heterostructure can exhibit photocatalytic activity enhancement only when TiO_2 is photoexcited. PdO nanoflake simply plays a role improving

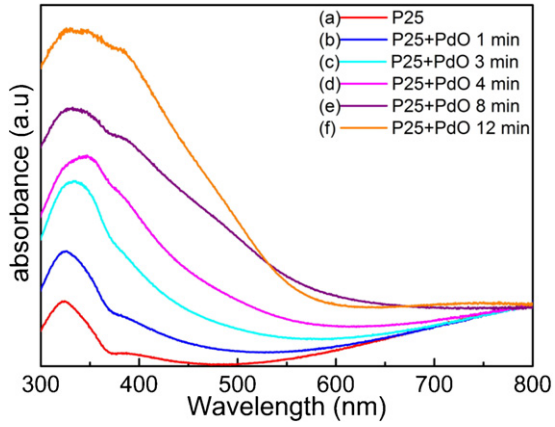

Fig. 5. UV–vis diffuse reflection absorption spectra of the as-prepared photocatalysts: (a) the P-25 sample, and the PdO/TiO_2 heterostructures prepared with different PdO deposition times: (b) 1 min, (c) 3 min, (d) 4 min, (e) 8 min, and (f) 12 min.

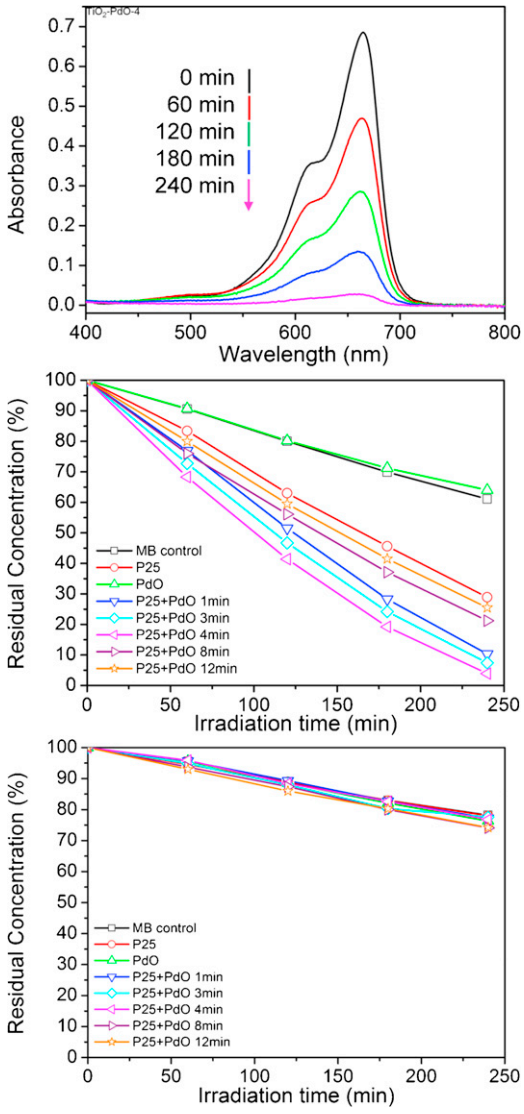

Fig. 6. (a) Absorption spectra of the MB solution in the presence of PdO–TiO_2-4 as a function of the UV light illumination time; the normalized MB concentration as a function of the illumination time in the presence of different photocatalysts under UV illumination (b) and under visible light illumination (c).

the charge separation in TiO_2 nanoparticles during photoexcitation. The enhanced photocatalytic activity of the PdO/TiO_2 heterostructure toward MB degradation under UV illumination can be ascribed to the fast charge transfer between the PdO nanoflake and theTiO_2 nanoparticle, which effectively separates the photogenerated e–h pairs and thus promotes the efficiency of photocatalytic MB decomposition on TiO_2 nanoparticles. In addition, much more photons can be harvested by the PdO/TiO_2 heterostructures compared with the P-25 sample because the extremely rough surface morphology due to the interconnected PdO nanoflakes can effectively reduce light reflection, thereby enhancing light absorption and thus photoexcitation of the heterostructures.

Photodegradation of organic chemicals catalyzed by TiO_2 has been extensively studied, and it is believed that organics photodegradation catalyzed by TiO_2 in aqueous solution occurs via complex reaction mechanisms, involving formation of different surface radicals and oxidation of the adsorbed organic compound [30,35,36]. Among various reaction intermediates, surface hydroxyl radicals ($OH^{\bullet}$), whose formation is primarily promoted by photogenerated carriers, play an important role in initiating organics photodecomposition. To facilitate MB decomposition, interfacial

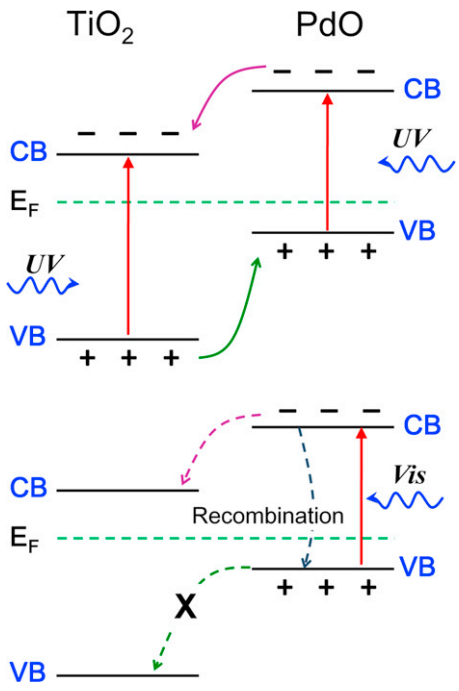

Fig. 7. Schematic energy band diagram of the PdO/TiO_2 heterostructure under (a) UV light illumination and (b) visible light illumination.

charge transfer between the TiO_2 nanoparticle and adsorbed reactant molecules forming active intermediates, such as $OH^{\bullet}$ radicals, must prevail over carrier recombination. Since the recombination lifetime (picoseconds to nanoseconds) is much shorter than the time required for the interfacial charge transfer reaction (microseconds to milliseconds) [9], e–h pair separation should be fast enough so that the interfacial charge transfer reaction can take place before the carrier recombination occurs. In the case of the PdO/TiO_2 heterostructure, the junction barrier developed between the two oxide semiconductors can enhance e–h pair separation. When a semiconductor is brought in contact with the other semiconductor of larger bandgap, band alignment leads to the formation of a staggered heterojunction as schematically illustrated by the band diagram in Fig. 7 [37–39]. Because of the large bandgap difference between PdO (~2.02 eV) and TiO_2 (~3.2 eV), the heterojunction formed by the p-type PdO and the n-type TiO_2 nanostructures has asymmetrical energy barriers at the interface. Upon UV–vis light illumination, electrons in the valence bands of the two semiconductors in the heterostructure are excited to the respective conduction bands, leaving holes in the valence bands. The energy barrier at the PdO/TiO_2 heterojunction will drive photogenerated electrons and holes to transport, respectively, to the conduction band of the TiO_2 and the valence band of the PdO. The built-in field at the heterojunction can promote fast separation of photogenerated e–h pairs, thereby greatly reduce carrier recombination [24,37,38]. When the separated carriers diffuse to the surface of the heterostructure, they react with adsorbed water and MB molecules, inducing a series of reactions which lead to MB decomposition.

Previous studies showed that photoresponse of TiO_2 can be extended to the visible light region when it forms heterojunction with a narrow bandgap semiconductor [23,24]. However, as shown in Fig. 6(c), the PdO–TiO_2 heterostructures do not exhibit perceivable photocatalytic activity toward MB degradation under visible light illumination. Upon visible light illumination, electrons photogenerated in the PdO nanoflake will be drifted to the conduction band of the TiO_2 nanoparticle due to the built-in field at the heterojunction, while photoexcited holes cannot be transferred to the valence band of TiO_2 nanoparticles because of the junction barrier (Fig. 7(b)). Since no photoexcitation occurs in TiO_2 nanoparticles under visible light illumination, there is no net charge flux between the two oxide semiconductors. Photogenerated e–h pairs quickly recombine in PdO nanoflakes, and thus MB photodecomposition cannot take place at the surface of TiO_2 nanoparticles. As a result, the PdO-TiO_2 heterostructure exhibits little photocatalytic activity toward the MB degradation under visible light illumination.

4. Conclusions

Ultrathin PdO nanoflakes were prepared by reactive sputter deposition to form a heterostructure with TiO_2 nanoparticles spin-coated on the SiO_2 substrate, and the photocatalytic performance of PdO/TiO_2 heterostructure toward MB decomposition was studied. Although the PdO nanoflake has little photocatalytic activity toward MB decomposition, it can improve the photocatalytic activity of TiO_2 under UV illumination. The photocatalytic activity of TiO_2 toward MB decomposition under UV–vis light illumination is greatly enhanced by the heterostructure. The enhancement of the photocatalytic activity is ascribed to that the junction barrier between the two oxide semiconductors facilitates the fast separation of electron–hole pairs photogenerated in the two oxides and, as a result, reduces the carrier recombination rate. The fast charge separation allows an efficient interfacial charge transfer between TiO_2 nanoparticles and adsorbed reactants, leading to the enhancement of MB photodecompsition. Under visible light illumination, the PdO/TiO_2 heterostructure exhibits little photocatalytic activity toward the MB decomposition although PdO can be photoexcited in the visible light range; the photocatalytic inactivity is due to that the junction barrier prohibits photogenerated holes in the PdO nanoflake from transporting to the TiO_2 nanoparticle, which cannot be photoexcited under visible light illumination.

Acknowledgements

This work was supported by the National Science Council of R.O.C (Taiwan) under contract no. NSC97-2221-E-009-016-MY3. We thank Professor Li Chang for helpful discussion and support in the PdO sputter deposition. Technical support from the National Nano Device Laboratories is also gratefully acknowledged.

References

[1] A.L. Linsebigler, G. Lu, J.T. Yates, Chemical Reviews 95 (1995) 735.
[2] C. Kang, L. Jing, T. Guo, H. Cui, J. Zhou, H. Fu, H. Lee, Journal of Physical Chemistry C 113 (2008) 1006.
[3] A. Fujishima, K. Honda, Nature 238 (1972) 37.
[4] N.G. Petrik, G.A. Kimmel, Journal of Physical Chemistry C 113 (2009) 4451.
[5] A. Valdeĭs, Z.W. Qu, G.L. Kroes, J. Rossmeisl, J.K. Nørskov, Journal of Physical Chemistry C 112 (2008) 9872.
[6] A.A. Ismail, D.W. Bahnemann, Green Chemistry 13 (2011) 428.
[7] A.A. Ismail, D.W. Bahnemann, J. Rathousky, V. Yarovyi, M. Wark, Journal of Materials Chemistry 21 (2011) 7802.
[8] A.A. Ismail, D.W. Bahnemann, L. Robben, V. Yarovyi, M. Wark, Chemistry of Materials 22 (2010) 108.
[9] M.R. Hoffmann, S.T. Martin, W. Choi, D.W. Bahnemann, Chemical Reviews 95 (1995) 69.
[10] E. Wang, W. Yang, Y. Cao, Journal of Physical Chemistry C 113 (2009) 20912.
[11] J. Choi, H. Park, M.R. Hoffmann, Journal Physical Chemistry C 114 (2009) 783.
[12] G.K. Mor, K. Shankar, M. Paulose, O.K. Varghese, C.A. Grimes, Nano Letters 6 (2005) 215.
[13] E. Thimsen, N. Rastgar, P. Biswas, Journal of Physical Chemistry C 112 (2008) 4134.
[14] H. Yu, S. Zhang, H. Zhao, B. Xue, P. Liu, G. Will, Journal of Physical Chemistry C 113 (2009) 16277.
[15] X. Han, Q. Kuang, M. Jin, Z. Xie, L. Zheng, Journal of the American Chemical Society 131 (2009) 3152.
[16] C. Burda, Y. Lou, X. Chen, A.C.S. Samia, J. Stout, J.L. Gole, Nano Letters 3 (2003) 1049.
[17] C. Chen, H. Bai, C. Chang, Journal of Physical Chemistry C 111 (2007) 15228.

[18] A.J. Cowan, J. Tang, W. Leng, J.R. Durrant, D.R. Klug, Journal of Physical Chemistry C 114 (2010) 4208.
[19] H. Huang, D. Li, Q. Lin, Y. Shao, W. Chen, Y. Hu, Y. Chen, X. Fu, Journal of Physical Chemistry C 113 (2009) 14264.
[20] X. Wang, J.C. Yu, H.Y. Yip, L. Wu, P.K. Wong, S.Y. Lai, Chemistry—A European Journal 11 (2005) 2997.
[21] S. Sato, J.M. White, Chemical Physics Letters 72 (1980) 83.
[22] D. Buso, J. Pacifico, A. Martucci, P. Mulvaney, Advanced Functional Materials 17 (2007) 347.
[23] S. Banerjee, S.K. Mohapatra, P.P. Das, M. Misra, Chemistry of Materials 20 (2008) 6784.
[24] L. Huang, F. Peng, H. Wang, H. Yu, Z. Li, Catalysis Communications 10 (2009) 1839.
[25] L. Yang, S. Luo, R. Liu, Q. Cai, Y. Xiao, S. Liu, F. Su, L. Wen, Journal of Physical Chemistry C 114 (2010) 4783.
[26] E.A. Sales, G. Bugli, A. Ensuque, M. De Jesus Mendes, F. Bozon-Verduraz, Physical Chemistry Chemical Physics 1 (1999) 491.
[27] T. Arai, T. Shima, T. Nakano, J. Tominaga, Thin Solid Films 515 (2007) 4774.
[28] J.R. McBride, K.C. Hass, W.H. Weber, Physical Review B 44 (1991) 5016.
[29] A.A. Ismail, Applied Catalysis B: Environmental 117–118 (2012) 67.
[30] A. Houas, H. Lachheb, M. Ksibi, E. Elaloui, C. Guillard, J.-M. Herrmann, Applied Catalysis B: Environmental 31 (2001) 145.
[31] C. Ratanatawanate, Y. Tao, K.J. Balkus, Journal of Physical Chemistry C 113 (2009) 10755.
[32] C.-J. Huang, F.-M. Pan, H.-Y. Chen, C. Li, Journal of Applied Physics 108 (2010) 053105.
[33] C.-J. Huang, F.-M. Pan, T.-C. Tzeng, C. Li, J.-T. Sheu, Journal of the Electrochemical Society 156 (2009) J28.
[34] J. Tschirch, R. Dillert, D. Bahnemann, B. Proft, A. Biedermann, B. Goer, Research on Chemical Intermediates 34 (2008) 381.
[35] S. Girish Kumar, L. Gomathi Devi, Journal of Physical Chemistry A 115 (2011) 13211.
[36] H. Gnaser, M.R. Savina, W.F. Calaway, C.E. Tripa, I.V. Veryovkin, M.J. Pellin, International Journal of Mass Spectrometry 245 (2005) 61.
[37] H. Chen, S. Chen, X. Quan, H. Yu, H. Zhao, Y. Zhang, Journal of Physical Chemistry C 112 (2008) 9285.
[38] M.P. Mikhailova, A.N. Titkov, Semiconductor Science and Technology 9 (1994) 1279.
[39] J. Zhang, H. Zhu, S. Zheng, F. Pan, T. Wang, ACS Applied Materials and Interfaces 1 (2009) 2111.